



ELSEVIER

Tectonophysics 321 (2000) 449–466

**TECTONOPHYSICS**

www.elsevier.com/locate/tecto

# Long and complex thermal history of the Song Chay metamorphic dome (Northern Vietnam) by multi-system geochronology

Françoise Roger <sup>a,\*</sup>, Philippe Hervé Leloup <sup>b</sup>, Marc Jolivet <sup>c</sup>, Robin Lacassin <sup>b</sup>, Phan Trong Trinh <sup>d</sup>, Maurice Brunel <sup>c</sup>, Diane Seward <sup>e</sup>

<sup>a</sup> *Laboratoire de Géochronologie, Univ. Paris 7–IPG Paris, CNRS–UMR 7578, 75252 Paris, France*

<sup>b</sup> *Laboratoire de Tectonique, Mécanique de la lithosphère IPG Paris, CNRS–UMR 7578, Paris, France*

<sup>c</sup> *GGP, Université Montpellier 2, CNRS UMR 5567, Montpellier, France*

<sup>d</sup> *Institute of Geological Sciences, NCNST, Hanoi, Viet Nam*

<sup>e</sup> *Geology Institute, ETH Zentrum, Sonneggstrasse 5, CH-8092 Zurich, Switzerland*

Received 9 March 1999; accepted for publication 7 March 2000

## Abstract

Multi-system geochronology was used to unravel the long and complex thermal history of the Song Chay range (Northern Vietnam), a high-grade granitic and metamorphic dome in the vicinity of the Cenozoic, Ailao Shan–Red River fault zone. It was considered to be Proterozoic South China basement, but its geological history was basically unknown. Scattered field observations suggest three episodes of high-temperature deformation: firstly at the time of granite emplacement, secondly a décollement with top to the north shear and thirdly anticlinal doming of the foliations formed during the two first stages. *P–T* estimates suggest that metamorphism coeval with the second deformation phase culminated at  $\sim 580^\circ\text{C}$  and  $\sim 4.5$  kbar ( $\sim 16$  km depth). Multi-system geochronology is applied to a two-micas granite sample, slightly deformed within the décollement. U/Pb dating of zircon yields an age of  $428 \pm 5$  Ma ( $\pm 2\sigma$ ) interpreted as the time of granite crystallization within the South China ‘Caledonian’ belt. Rb/Sr on white micas and biotite yields ages of  $206 \pm 10$  Ma and  $176 \pm 5.3$  Ma, respectively ( $2\sigma$ ), whereas  $^{39}\text{Ar}/^{40}\text{Ar}$  ages of the same minerals are  $210 \pm 9$  and  $190 \pm 8$  Ma ( $2\sigma$ ). These ages suggest an Upper Triassic episode of rapid cooling interpreted as due to doming a few million years after the end of movement on the décollement. The K-feldspar irregular  $^{39}\text{Ar}/^{40}\text{Ar}$  age spectrum can, to the first order, be explained by a cooling history with two episodes of rapid cooling: one at  $\sim 140$  Ma and a second around 41 to 25 Ma. Apatite fission tracks central age ( $33.6 \pm 3.6$  Ma,  $1\sigma$ ) confirms a Tertiary rapid cooling event interpreted as the final exhumation of the Song Chay dome. © 2000 Elsevier Science B.V. All rights reserved.

*Keywords:* Caledonian orogeny; geochronology; Indosinian orogeny; *P–T–t* paths; tectonics; thermochronology

## 1. Introduction

Deciphering complex geological histories has always been a challenge in geology. Geo-

chronology allows us to assess this problem by giving constraints on the timing of crystallization and thermal evolution of plutonic rocks. In this paper the joint use of several geochronological methods on several minerals within a single orthogneiss sample allows us to define most of the long and complex temperature history, from gran-

\* Corresponding author.

*E-mail address:* roger@ipgp.jussieu.fr (F. Roger)

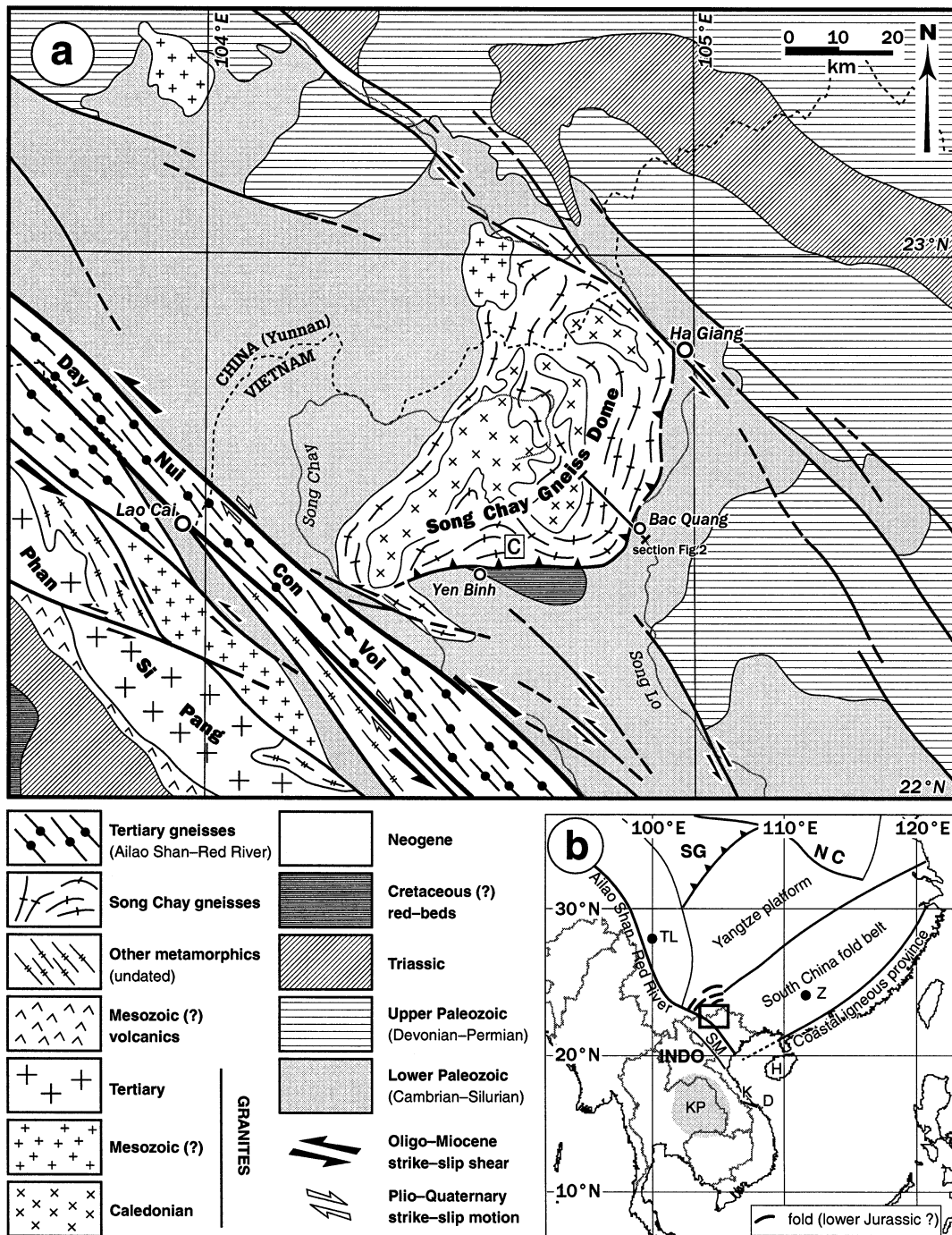


Fig. 1. (a) Structural setting of the Song Chay dome. Cross-section of Fig. 2 and zone c are located. (b) Sketch map of SE Asia showing location of area studied in Vietnam. SG: Songpan Garze; NC: North China Block; Indo: Indochina; Yangtze platform + South China fold belt + Coastal igneous province: South China Block; Z: Zhuguangshan batholith; TL: Tiger-leap folded décollement; D: Da Nang; K: Khe Sanh; SM: Song Ma anticlinorium; KP: Khorat plateau; H: Hainan island.

ite emplacement to near-surface exhumation, of the Song Chay metamorphic dome (Northern Vietnam) (Fig. 1). The methods used are the following: U/Pb on zircon; Rb/Sr on K-feldspar, whole rock, biotite and muscovite;  $^{39}\text{Ar}/^{40}\text{Ar}$  on biotite, muscovite and K-feldspar; and fission tracks on zircon and apatite. These radiogenic systems have closure temperatures spanning from more than 800°C to less than 110°C. Combined together they define a temperature history lasting for more than 400 m.y. When complemented by structural and petrographic observations such a temperature history helps us to propose a first-order pressure–temperature–time–deformation path ( $P$ – $T$ – $t$ – $D$ ). In this area, where reliable geochronological data are scarce, such a study provides important constraints to answer several important questions, such as: when did the Song Chay protolith originate? When was it affected by penetrative ductile deformation? Was the Song Chay dome affected by a penetrative tectonometamorphic event during left-lateral shearing along the Ailao Shan–Red River shear zone (ASRR) only a few kilometres away?

## 2. The Song Chay dome geological setting

The northern part of Vietnam is cut by the NW–SE-striking ASRR that separates the South China and Indochina blocks. Major left-lateral ductile shear occurred along this zone in the Oligo-Miocene as Indochina was extruded several hundreds of kilometres towards the southeast (e.g. Tapponnier et al., 1986, 1990; Yang and Besse, 1993; Leloup et al., 1995). These sheared high-grade rocks have been subsequently exhumed and are presently exposed in the Day Nui Con Voi range (Fig. 1a). North of this zone, in the Song Chay range (maximum relief 2400 m), is the Song Chay high-grade gneiss and granite complex (Fig. 1). This complex is the largest one in the southwestern South China block and straddles the Vietnam–Yunnan border. It is chiefly composed of migmatites, porphyroid granites and augen-gneisses resulting from the deformation of these granites (Deprat, 1915; Staritskiy et al., 1973; Tran Van Tri, 1979). These rocks form a 40 km

wide dome and have been considered to be of Precambrian age (e.g. Deprat, 1915; Izokh et al., 1964; Tran Van Tri, 1979). Radiometric data for the Song Chay gneisses are reported to range from 2652 to 625 Ma with little information on the methods used and no error ranges (Tran Van Tri, 1979; Hutchinson, 1989, p. 147). The Song Chay dome was therefore considered to represent exhumed basement of the South China block (e.g. Fromaget, 1941; Hutchinson, 1989).

Between Yen Binh and Bac Quang, nearly vertical to steeply dipping (70 to 90°) slabs of paragneisses, migmatites and augen-gneisses mark the southern and eastern flanks of the Song Chay dome that show particularly steep topographic gradients [Fig. 1, Fig. 2 (zones a and c), Fig. 3a]. These slabs are parallel to the foliation of the rocks, and to the border of the gneiss dome. East of Yen Binh, the steep east–west-trending Yen Binh fault (Fromaget, 1941) overthrusts these gneisses on a syncline of red beds series, possibly of Cretaceous age (General Geological Department, 1973; General Department of Mines and Geology, 1988) (Fig. 1). This fault, which marks the base of the mountain front, presents a sharp trace on Landsat and SPOT satellite images, suggesting that it could be a recent, or still active, thrust.

Granite and derived gneisses are exposed in the core of the Song Chay dome (Deprat, 1915; General Geological Department, 1973; Staritskiy et al., 1973). Along the section from Bac Quang to Ta Quan (Fig. 2), granites are generally transformed into moderately deformed gneisses bearing large (1–10 cm) feldspar augens (Fig. 3c and d). Zones of undeformed granite (Fig. 3b) as well as metre-scale mylonitic bands occur within these augen-gneisses. Within the dome, the foliation is flat, slightly dipping 0–20° toward the SE (zone b, Fig. 2). These flat foliation planes generally bear a stretching lineation that, on average, strikes N005° (zone b, Fig. 2). In these rocks, shear sense indicators, such as C/S structures or asymmetric feldspar porphyroclasts, imply shearing towards the north on flat-lying shear planes (Fig. 3c and d). Approaching the southeastern boundary of the dome, the foliation and lineation become steep (Fig. 2), with foliation planes dipping 70–90° SE

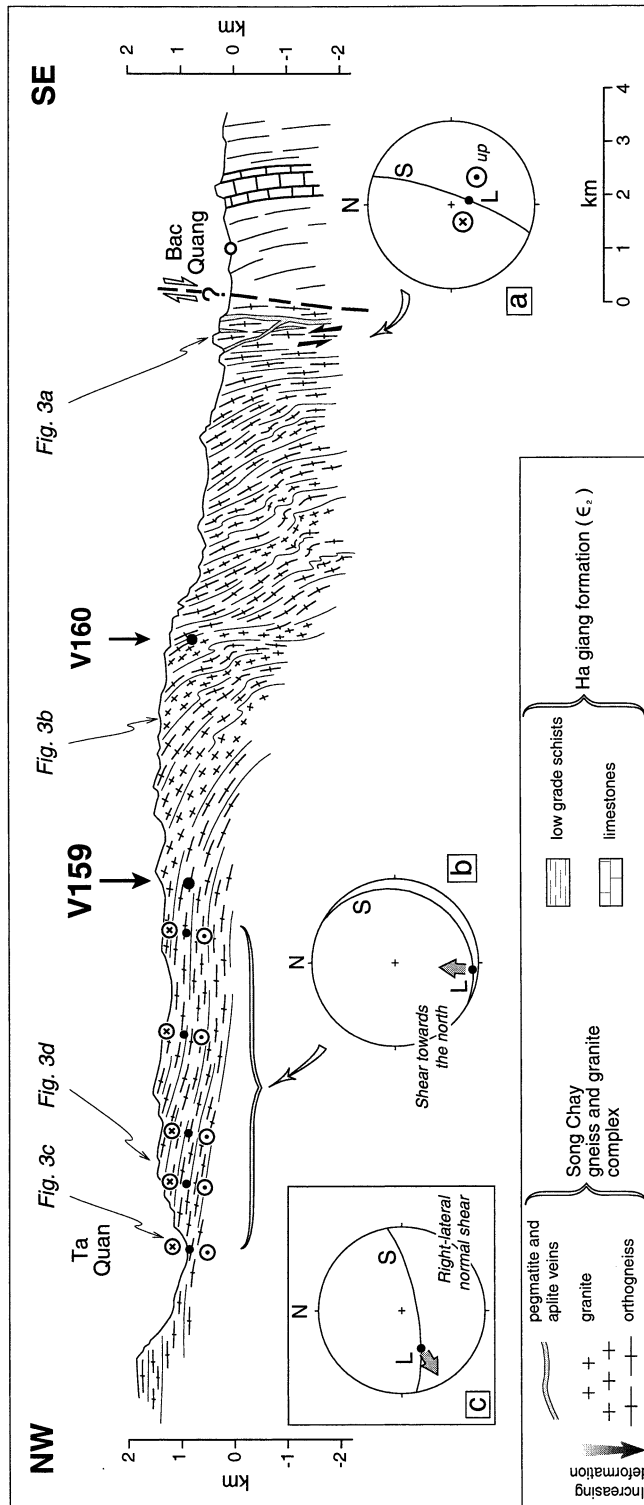


Fig. 2. Structure of the Song Chay dome. Cross-section Bac Quang-Ta Quan drawn from field observations. Small diagrams are lower hemisphere Schmidt projections of the foliation and lineation in zones a (dome core), b (dome east flank) and c (dome south flank, see location on Fig. 1a).

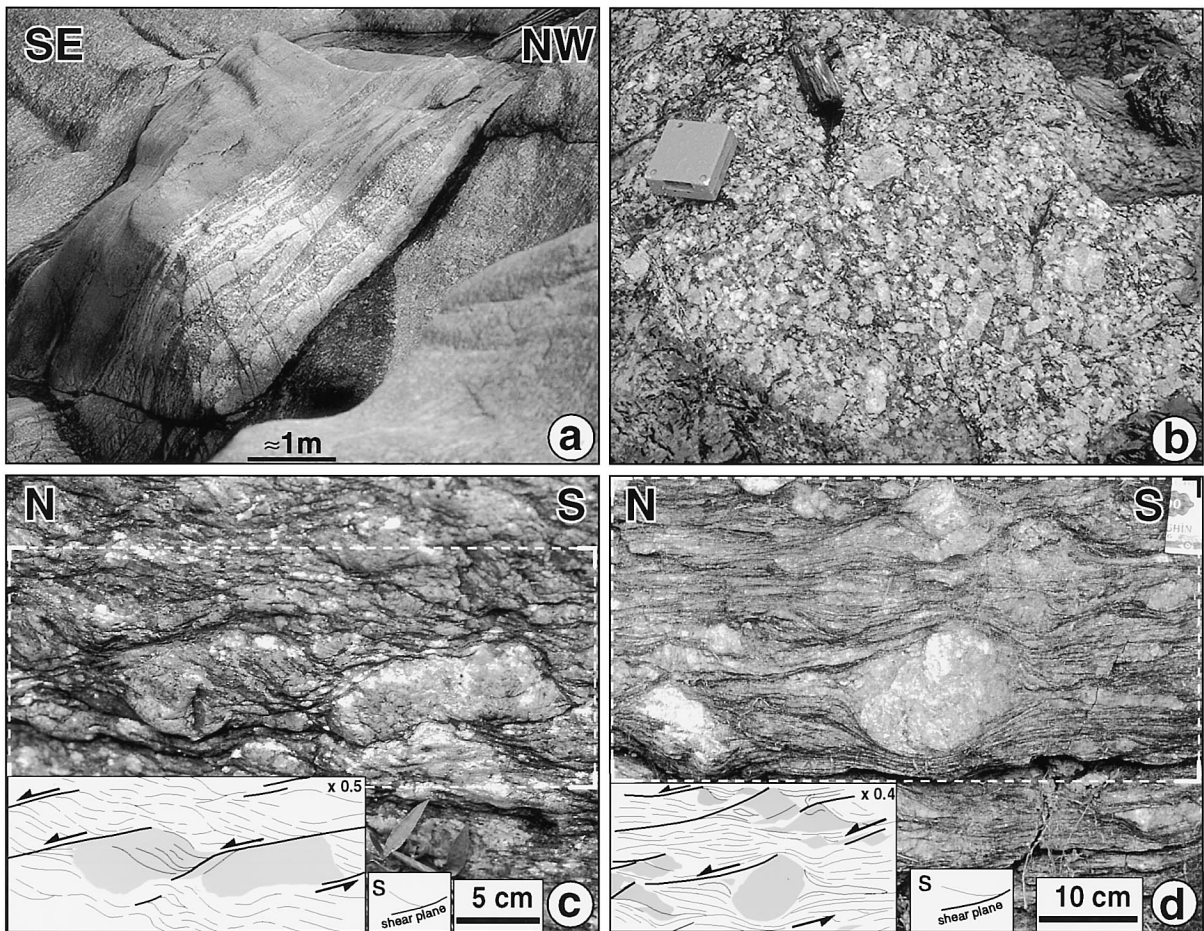


Fig. 3. Typical rock facies of the Song Chay dome. See Fig. 2 for location. (a) Gneiss from the dome east flank with deformed and cross-cutting aplitic dykes. (b) Undeformed granite, compass gives scale. (c) and (d) Deformed orthogneiss from the dome core showing top to the north shear criteria.

and lineations with a pitch of  $\sim 70^\circ$  S (zone a, Fig. 2). In this region, shear senses are less clear than in the dome core but suggest that the south-east block is moving upwards. Near the southern border of the dome, northeast of Yen Binh (Fig. 1), steeply south-dipping foliation planes bear lineations with pitches between  $35$  and  $50^\circ$  west and shear criteria compatible with normal right-lateral shearing (zone c, Fig. 2).

Most deformations occurred in the ductile field at relatively high temperature, above  $300^\circ\text{C}$  (quartz recrystallization, stability of biotite). Along the eastern and southern border of the dome (zones a and c), the presence of both deformed and few

cross-cutting aplitic and pegmatitic veins (Fig. 3a) suggests that deformation was contemporaneous with magmatism. In the core, where foliations are flat (zone b) no cross-cutting dikes are found. In this zone, large K-feldspar porphyroclasts are preserved, and muscovite is found crystallized in shear planes which suggests that deformation occurred in low amphibolite facies conditions, probably not much above  $500^\circ\text{C}$  (Gapais 1989; Le Goff and Ballèvre, 1990).

Along the Bac Quang–Ta Quan section, a sample of garnet micaschist (V160, Fig. 2) yielded  $P$ – $T$  estimates using thermo-barometers based on composition equilibria between co-genetic miner-

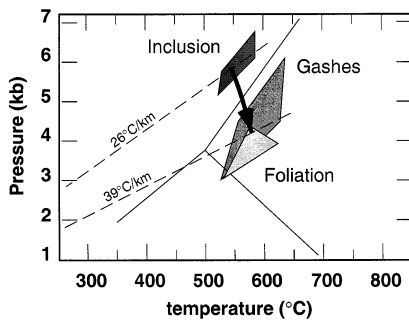


Fig. 4. V160  $P$ - $T$  path. Data from thermo-barometers based on composition equilibria between co-genetic minerals; see text for details. Average thermal gradients are given for comparison.

als. The sample foliation is mainly underlined by biotites but also contains quartz, plagioclase (An30–40) and muscovite. This foliation wraps around garnet porphyroclasts that contain biotite and plagioclase (An20) inclusions, and are crosscut by tension gashes containing recrystallized plagioclases (An30–40) and biotites. Garnet–biotite (Hodges and Spear, 1982) and garnet–biotite–plagioclase (Hoisch, 1991) thermo-barometers suggest a pressure of  $\sim 6$  kbar ( $\sim 21$  km) and a temperature of  $\sim 550^\circ\text{C}$  for the inclusions, whereas they indicate a lower pressure ( $\sim 4.5$  kbar or  $\sim 16$  km) and a slightly higher temperature ( $580^\circ\text{C}$ ) for the tension gashes (Fig. 4). The same thermo-barometers, together with the garnet–biotite–plagioclase–muscovite equilibrium (Powell and Holland, 1988), suggest a pressure of  $\sim 3.8$  kbar ( $\sim 14$  km) and a temperature of  $\sim 575^\circ\text{C}$  at the time of the foliation development (Fig. 4). We suggest that the foliation and the tension gashes within the garnet both results from the same progressive deformation at  $\sim 15$  km depth and  $\sim 580^\circ\text{C}$  (average thermal gradient of  $39^\circ\text{C}/\text{km}$ ) at the expense of garnets formed approximately 6 km deeper under a lower average thermal gradient ( $\sim 26^\circ\text{C}/\text{km}$ ). This progressive deformation probably resulted from the top to the north shearing described in zone b.

### 3. Multi-system geochronology

To constrain the  $P$ - $T$ - $t$  path of the Song Chay dome we carried out a multi-system geochronology

study of sample V159 from the Bac Quang–Ta Quan section (Figs. 1 and 2). The sample is a deformed orthogneiss containing large microcline porphyroclasts ( $\sim 1$  cm), biotites and white micas. Zircon and apatite occur as accessory minerals.

#### 3.1. $U$ - $Pb$ analyses

The zircon  $U/Pb$  analytical results are reported in Table 1, and the seven fractions plotted on the concordia diagram (Fig. 5). Four experimental points with a degree of discordance less than 8% have a mean  $^{207}\text{Pb}/^{206}\text{Pb}$  age of  $425 \pm 3$  Ma. A linear regression including the seven fractions yields an upper intercept age of  $428 \pm 5$  Ma ( $\pm 2\sigma$ ) and a lower intercept of  $51 \pm 23$  Ma (M.S.W.D. = 0.92). Regarding the value of the closure temperature of at least  $800^\circ\text{C}$  for the  $U/Pb$  system in the zircon (Pidgeon and Aftalion, 1978; Mezger, 1990; Dahl, 1997; Lee et al., 1997), and the position of points close to the intercept, the age of  $428 \pm 5$  Ma is assumed to represent the age of granite emplacement.

#### 3.2. $Rb$ - $Sr$ analyses

Whole rock, K-feldspar, three different size fractions of biotite and four different size fractions

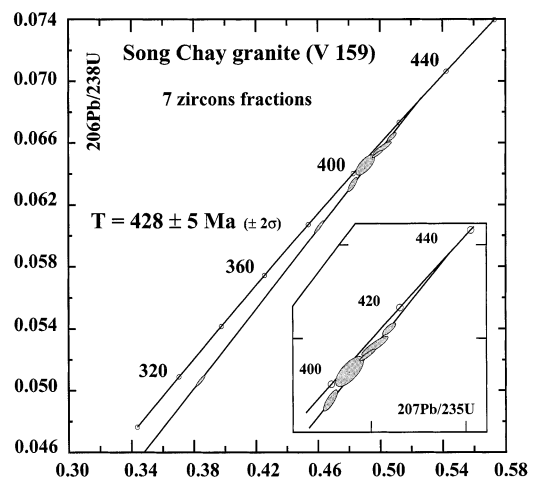


Fig. 5. Concordia diagram for zircon from Song Chay granite (V159).

Table 1  
U/Pb analytical results for zircon from the Song Chay granite (V159)<sup>a</sup>

Song Chay granite (V159) <sup>b</sup>	Weight (mg)	Concentrations (ppm)		Measured <sup>206</sup> Pb/ <sup>204</sup> Pb	Atomic ratios <sup>c</sup>			Apparent ages (Ma)		
		U	Pb		<sup>206</sup> Pb*/ <sub>238U</sub>	<sup>207</sup> Pb*/ <sub>235U</sub>	<sup>207</sup> Pb*/ <sub>206Pb*</sub>	<sup>206</sup> Pb*/ <sub>238U</sub>	<sup>206</sup> Pb*/ <sub>235U</sub>	<sup>206</sup> Pb*/ <sub>206Pb*</sub>
<i>Zircons</i>										
1: Nab, small, needles, pink, Trp	0.0154	362	22.1	675	0.063 31	0.482 40	0.055 26	395.7	399.7	422.9
2: Ab, medium, pink, Trp	0.0525	590	37.4	1764	0.065 67	0.501 54	0.055 39	410.0	412.7	428.0
3: Ab, medium, pink, Trp	0.0266	678	41.8	614	0.064 56	0.490 63	0.055 11	403.3	405.3	416.8
4: Nab, medium, pink, Trp	0.1856	600	34.7	9128	0.060 56	0.460 80	0.055 18	379.0	384.8	419.7
5: Nab, medium, pink, Trp	0.0131	612	31	2113	0.050 64	0.384 31	0.055 04	318.5	330.2	413.7
6: Ab, medium, pink, Trp	0.0162	944	59.5	2057	0.066 39	0.507 60	0.055 45	414.4	416.8	430.4
7: Ab, large, pink, Trp	0.0853	579	35.8	14732	0.065 28	0.498 35	0.055 37	407.6	410.6	427.1

<sup>a</sup> The asterisk indicates radiogenic element.

<sup>b</sup> The individual analyses were performed on euhedral, unbroken, crack-free from the best quality grains of the population Small: grains 50–100 μm in length; medium: 100–150 μm in length; large > 150 μm in length; Nab: not abraded; Ab: abraded; Trp: transparent.

<sup>c</sup> Ratio corrected for mass discrimination ( $\pm 0.1\%/amu$  for Pb and U), spike contribution, 15 pg of Pb blank, 1 pg of U blank and initial common Pb as determined on K-feldspar from the same rock. These values are for <sup>206</sup>Pb/<sup>204</sup>Pb = 18.05, <sup>207</sup>Pb/<sup>204</sup>Pb = 15.59 and <sup>208</sup>Pb/<sup>204</sup>Pb = 37.85.

of muscovite were analysed for Rb/Sr (Table 2). In an (<sup>87</sup>Sr/<sup>86</sup>Sr) = *f*(<sup>87</sup>Rb/<sup>86</sup>Sr) diagram, two linear arrays are defined when a set of grains is regressed: one is the muscovite fractions, K-feldspar and whole-rock analyses; the second is biotite fractions, K-feldspar and whole-rock analyses. The data from the two slopes yield 206 ± 10 Ma ( $\pm 2\sigma$ ) with an initial <sup>87</sup>Sr/<sup>86</sup>Sr ratio of 0.7369 ± 0.0059 (muscovites) and 176 ± 5.3 Ma ( $\pm 2\sigma$ ) with an initial Sr ratio of 0.7377 ± 0.0003 (biotites) (Fig. 6). The two initial <sup>87</sup>Sr/<sup>86</sup>Sr ratios for biotite and muscovite are similar and highly radiogenic, suggesting that the major source lithology of the granite was a

highly evolved continental crust. The temperature of metamorphism (~580°C) is well above the closure temperature of Rb/Sr in muscovite (450–500°C, Purdy and Jäger, 1976; Cliff, 1985), thus 206 ± 10 Ma is interpreted as a minimum age (cooling age) for the metamorphic event.

### 3.3. Ar/Ar analyses

Biotites and white micas yield quite flat <sup>39</sup>Ar/<sup>40</sup>Ar age spectra with respective weighted mean plateau ages of 190 ± 8 Ma ( $\pm 2\sigma$ , seven steps used over ten representing 98.4% of gas) and 210 ±

Table 2

Rb/Sr analytical results for whole rock, K-feldspars, muscovites and biotites. Analytical uncertainties are  $\pm 2\%$  for <sup>87</sup>Rb/<sup>86</sup>Sr, and for <sup>87</sup>Sr/<sup>86</sup>Sr; they are given on the last digit of the values measured. <sup>87</sup>Sr/<sup>86</sup>Sr is normalized to <sup>86</sup>Sr/<sup>88</sup>Sr = 0.1194

Sample: V159	Rb (ppm)	Sr (ppm)	<sup>87</sup> Rb/ <sup>86</sup> Sr	<sup>87</sup> Sr/ <sup>86</sup> Sr ( $\pm 2\sigma$ )
Whole rock	159.7	65.3	7.20	0.753 53 ± 7
Feldspar	173	94.8	5.37	0.752 19 ± 2
Biotite 1 (400/600 μm)	636.5	6.3	319.9	1.529 85 ± 15
Biotite 2 (600/800 μm)	825.4	7.5	353.2	1.638 86 ± 6
Biotite 3 (> 800 μm)	619	3.3	633.8	2.312 41 ± 42
Muscovite 1 (< 400 μm)	292.9	8.5	104.8	1.041 55 ± 4
Muscovite 2 (400/600 μm)	211.9	7.4	86.9	0.998 82 ± 4
Muscovite 3 (400/600 μm)	305.8	8.7	95.8	1.022 65 ± 6
Muscovite 4 (600/800 μm)	248.4	5.7	112.3	1.057 07 ± 5

Table 3  
Argon results<sup>a</sup>

Temp (°C)	Time (min)	<sup>40</sup> Ar/ <sup>39</sup> Ar	<sup>38</sup> Ar/ <sup>39</sup> Ar	<sup>37</sup> Ar/ <sup>39</sup> Ar	<sup>36</sup> Ar/ <sup>39</sup> Ar 10 <sup>-3</sup>	<sup>39</sup> Ar 10 <sup>-15</sup> mol	% <sup>39</sup> Ar released	% <sup>40</sup> Ar*	<sup>40</sup> Ar*/ <sup>39</sup> Ar <sub>K</sub>	Age (Ma)	±1σ (Ma)
<b>V159</b>		<b>biotite</b>		<i>J</i> = 0.008 3690		wt = 8.15 mg					
500	15	23.180	0.030 762	0.104 018	49.404 89	1.885 391	0.43	38.24	8.865	129.52	2.55
600	14	14.671	0.021 592	0.008 116	5.716 872	24.391 96	5.99	88.70	13.014	187.09	3.77
700	15	14.360	0.020 802	0.003 213	2.649 802	179.1627	46.88	94.65	13.592	194.96	3.99
750	26	13.499	0.020 118	0.002 453	0.253 579	92.215 39	67.92	99.46	13.426	192.70	3.83
800	25	13.367	0.020 652	0.008 487	0.471 816	22.598 52	73.08	98.98	13.231	190.05	3.80
900	15	14.143	0.021 000	0.045 720	3.680 495	23.592 27	78.46	92.48	13.081	188.01	3.76
1000	24	13.359	0.020 531	0.027 453	1.197 234	69.757 15	94.38	97.42	13.015	187.11	3.74
1100	17	13.740	0.020 508	0.114 575	1.276 259	19.457 04	98.82	97.39	13.385	192.15	3.81
1200	17	13.272	0.019 967	0.113 579	1.960 638	3.541 909	99.63	95.80	12.718	183.04	3.66
1400	19	7.284	0.019 843	0.105 148	8.514 047	1.627 748	100	66.25	4.826	71.67	3.29
<b>V159</b>		<b>muscovite</b>		<i>J</i> = 0.008 394 5		wt = 4.08 mg					
400	15	259.775	0.180 766	0.000 000	858.1591	0.012 828 4	0.01	4.20	10.909	158.08	70.41
500	16	21.239	0.025 900	0.066 609	35.260 98	0.253 931 1	0.10	51.89	11.022	159.65	5.10
600	15	17.778	0.021 052	0.035 820	14.5193	1.2193	0.54	76.34	13.572	194.65	3.80
700	17	40.085	0.035 785	0.035 093	90.355 23	13.019 25	5.24	34.64	13.886	198.92	5.50
750	14	15.708	0.017 794	0.006 091	3.380 246	26.332 77	14.76	93.76	14.729	210.31	4.12
800	18	14.906	0.017 417	0.003 630	0.666 613	72.123 44	40.84	98.71	14.713	210.10	4.16
850	20	14.719	0.017 336	0.003 929	0.424 681	85.179 56	71.63	99.17	14.597	208.53	4.19
900	18	14.950	0.017 122	0.021 613	1.072 175	17.864 02	78.09	97.93	14.642	209.14	4.15
950	22	15.068	0.017 296	0.032 053	1.648 778	11.138 16	82.12	96.85	14.594	208.49	4.10
1000	18	14.857	0.016 729	0.024 502	0.557 054	5.111 757	83.96	98.93	14.698	209.91	4.24
1100	25	15.243	0.016 706	0.007 115	0.428 977	24.9073 8	92.97	99.19	15.120	215.58	4.06
1200	24	14.674	0.017 704	0.009 446	3.0562	5.056 082	94.80	93.97	13.789	197.60	4.15
1400	30	5.669	0.019 315	0.011 327	6.048 216	12.789 15	99.42	69.08	3.916	58.36	1.44
1400	40	14.661	0.024 893	0.024 631	40.100 39	1.604 453	100	20.70	3.034	45.38	5.57
<b>V159</b>		<b>Kf</b>		<i>J</i> = 0.013 490 0		wt = 21.87 mg					
400	15	42.814	0.053 843	0.022 307	122.1749	0.694 270 4	0.02	17.24	7.380	171.23	3.73
400	20	14.290	0.028 715	0.019 107	38.362 89	0.729 154 9	0.05	22.12	3.161	75.34	2.82
450	15	4.941	0.022 558	0.012 369	7.826 935	3.330 454	0.16	53.96	2.666	63.75	1.31
450	20	2.479	0.018 905	0.010 734	2.931 627	4.947 223	0.32	65.50	1.624	39.10	0.85
501	16	2.492	0.018 122	0.013 849	1.060 712	15.585 34	0.85	87.46	2.180	52.30	1.03
501	20	1.625	0.017 669	0.023 148	0.557 646	15.888 61	1.38	89.77	1.459	35.17	0.70
551	15	2.428	0.017 617	0.031 649	0.328 702	33.890 67	2.51	95.91	2.329	55.82	1.10
551	20	2.102	0.017 553	0.019 589	0.248 399	35.550 03	3.70	96.35	2.025	48.64	0.96
602	15	2.888	0.017 670	0.016 868	0.248 233	51.931 73	5.44	97.34	2.812	67.18	1.32
603	26	2.977	0.017 709	0.010 174	0.192 829	63.423 53	7.57	97.94	2.916	69.62	1.38
652	17	3.536	0.017 764	0.007 714	0.348 202	91.909 46	10.65	96.99	3.429	81.60	1.60
650	25	3.620	0.017 580	0.003 956	0.129 744	74.2856	13.14	98.80	3.576	85.02	1.67
700	20	3.938	0.017 352	0.003 845	0.159 081	107.9932	16.76	98.68	3.886	92.19	1.86
743	31	4.688	0.017 403	0.003 630	0.268 176	159.0389	22.08	98.22	4.604	108.73	2.13
803	17	5.117	0.017 386	0.004 033	0.380 648	99.631 09	25.42	97.73	5.001	117.80	2.32
804	18	5.074	0.017 352	0.003 939	0.419 251	50.669 04	27.12	97.49	4.947	116.55	2.29
800	32	5.295	0.017 618	0.003 548	0.536 764	44.916 38	28.63	96.95	5.134	120.81	2.34
800	60	5.514	0.017 531	0.004 016	0.644 166	54.129 84	30.44	96.51	5.321	125.08	2.46
800	87	5.998	0.017 628	0.003 712	0.792 269	63.706 76	32.57	96.07	5.762	135.06	2.62
700	20	7.992	0.014 539	0.000 000	1.6144	1.947 413	32.64	94.07	7.518	174.28	3.43
750	22	6.795	0.017 312	0.004 069	1.048 774	5.202 672	32.81	95.44	6.485	151.32	2.92
800	20	6.385	0.017 513	0.004 283	0.875 796	13.568 72	33.27	95.93	6.126	143.26	2.75
852	16	6.378	0.017 680	0.004 307	0.962 475	29.395 36	34.25	95.53	6.093	142.52	2.80
900	15	6.433	0.017 776	0.004 867	0.745 854	74.006 91	36.73	96.55	6.211	145.16	2.80

Table 3 (continued)

Temp (°C)	Time (min)	<sup>40</sup> Ar/ <sup>39</sup> Ar	<sup>38</sup> Ar/ <sup>39</sup> Ar	<sup>37</sup> Ar/ <sup>39</sup> Ar	<sup>36</sup> Ar/ <sup>39</sup> Ar 10 <sup>-3</sup>	<sup>39</sup> Ar 10 <sup>-15</sup> mol	% <sup>39</sup> Ar released	% <sup>40</sup> Ar*	<sup>40</sup> Ar*/ <sup>39</sup> Ar <sub>K</sub>	Age (Ma)	± 1σ (Ma)
950	15	6.272	0.017182	0.004144	0.556975	161.3086	42.14	97.33	6.105	142.78	2.80
1000	18	6.092	0.017214	0.004099	0.454472	233.2425	49.95	97.74	5.954	139.40	2.70
1000	30	5.873	0.017169	0.003769	0.367034	130.7835	54.33	98.09	5.761	135.03	2.64
1000	50	6.048	0.017398	0.003805	0.361336	122.959	58.45	98.17	5.938	139.02	2.70
1000	108	6.097	0.017410	0.003429	0.312298	111.3823	62.18	98.42	6.001	140.45	2.80
21	449	7.443	0.019024	0.004332	1.430273	5.566	62.37	94.35	7.023	163.31	7.44
900	28	6.316	0.017013	0.004090	0.000000	4.554	62.52	99.90	6.310	147.40	2.86
950	20	6.418	0.017229	0.002926	0.058313	7.616	62.78	99.65	6.395	149.30	2.89
1000	21	6.139	0.017655	0.003995	0.147171	14.671	63.27	99.21	6.091	142.47	2.79
1050	15	6.715	0.017590	0.004238	0.325341	28.647	64.23	98.51	6.615	154.23	2.97
1100	18	6.955	0.017690	0.004459	0.377858	80.582	66.93	98.34	6.840	159.24	3.05
1146	17	7.135	0.017272	0.003892	0.403253	117.304	70.86	98.28	7.013	163.08	3.13
1200	17	7.756	0.017431	0.003291	0.508738	196.001	77.43	98.02	7.603	176.15	3.36
1200	21	7.590	0.017363	0.003195	0.574958	108.032	81.05	97.73	7.418	172.06	3.33
1200	30	7.369	0.017633	0.003806	0.644655	88.401	84.01	97.38	7.177	166.73	3.23
1200	45	7.196	0.017636	0.003465	0.678009	94.810	87.19	97.19	6.993	162.65	3.12
1200	61	6.872	0.017678	0.002630	0.646236	93.194	90.31	97.19	6.678	155.63	2.99
1300	15	6.634	0.017179	0.002349	0.424359	142.885	95.10	98.06	6.505	151.77	2.95
1300	20	6.333	0.017105	0.002664	0.406224	81.589	97.83	98.05	6.209	145.13	2.81
1400	20	6.370	0.017513	0.003449	0.600425	53.366	99.62	97.18	6.190	144.70	2.80
1400	31	8.030	0.017741	0.001961	4.808982	8.158	99.89	82.56	6.629	154.54	3.16
1400	30	11.089	0.019922	0.002414	15.86558	3.239	100	58.46	6.482	151.25	4.42

<sup>a</sup> Asterisk indicates radiogenic element; <sup>39</sup>Ar<sub>K</sub>: <sup>39</sup>Ar produced by <sup>39</sup>K during irradiation.

9 Ma (±2σ, six steps used over 14 representing 78.5% of gas), (Table 3, Fig. 7a). Corresponding inverse isochron plots do not reveal any significant excess argon. The K-feldspars show a much more irregular age spectrum (Fig. 7a). Ages range from

Cenozoic at low temperatures (minimum age of 35 Ma) to a flatter portion at ~140 Ma among 33 and 62% of gas release preceded by a peak at ~174 Ma. The last 33% of gas, released above the melting temperature of K-feldspar during the measurement (~1150°C), is marked by an age culminating at 176 Ma followed by decreasing ages down to 145 Ma, strongly suggesting excess argon in this part of the age spectrum. Given its irregularities, this age spectrum is difficult to interpret. For example, we have no direct evidence that the apparent ages around 140 Ma of the age spectrum are not affected by excess argon. However, the ages of this spectrum are not anomalous as they fall between the biotite Rb/Sr and the central apatite track (see below) ages. Bearing in mind the above uncertainties on the K-feldspar data, we tried to determine if the shape of the K-feldspar age spectrum could be explained by a diffusion model.

As is often the case for microcline K-feldspars, to obtain sample diffusion characteristics is not trivial, especially for the very low and high furnace temperatures (≤500°C and ≥1100°C). An automated

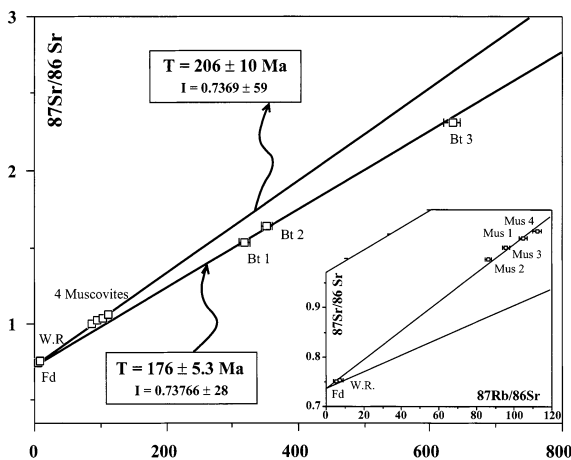


Fig. 6. Rb/Sr isochron diagram for whole rock, K-feldspar, muscovites and biotites from the Song Chay granite (V159).

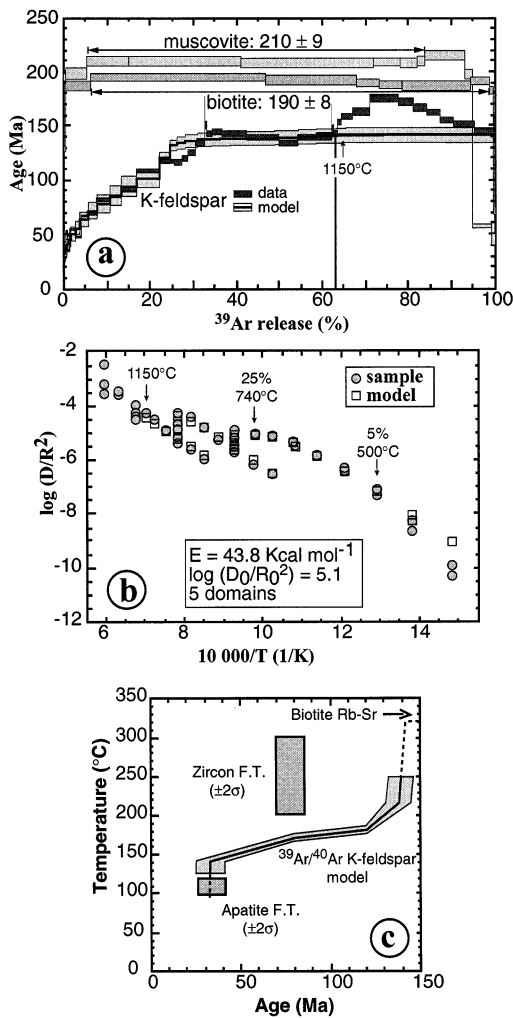


Fig. 7. V159  $^{39}\text{Ar}/^{40}\text{Ar}$  results. (a) Biotite, muscovite and K-feldspar age spectra. Black line and light grey shading correspond to model age spectra obtained using diffusion parameters shown in (b) and cooling histories shown in (c). (b) K-feldspar Arrhenius plot. Experimental data are filled circles and diffusion model is open squares. (c) Model K-feldspar cooling histories. Black line corresponds to best-fit solution [black age model spectrum on (a)], whereas grey area corresponds to other possible cooling histories [light grey shading on (a)]. Dashed portions of cooling history were used for calculations but are not directly constrained by the  $\text{Ar}^{39}/\text{Ar}^{40}$  data. Age-closure temperature range of zircon and apatite fission track ( $\pm 2\sigma$ ) are shown for comparison.

inverse process (program ‘auto.arr’ by O. Lovera) yields the domain distribution that best fits the experimental data, assuming that diffusion is the

only argon transport mechanism (e.g. Lovera et al., 1989, 1997). This solution assumes five diffusion domains with  $E=43.75$  kcal/mol and  $\log(D_0/r_0^2)=5$ . It gives a good fit to the data between 5 and 22% of gas release that correspond to the spectrum rapid rise in age (Fig. 7b). Such a model does not intend to fit the data obtained above  $1150^\circ\text{C}$ , i.e. the temperature at which the sample melts.

Taking these diffusion characteristics, it is possible to model the theoretical age spectrum corresponding to a given cooling history (e.g. Lovera et al., 1989, 1991; Lovera, 1992). Many cooling histories can yield model age spectra approximately fitting the V159 age spectrum. These cooling histories are of two kinds: relatively simple histories showing continuous cooling, and more complex ones presenting a re-heating event. In the absence of any independent evidence for a late re-heating event, we determined a set of continuous cooling histories that fit best the V159 data. All these cooling histories (grey array on Fig. 7c) show an Upper Jurassic rapid cooling starting around 140 Ma ago, and a Tertiary cooling starting between 41 to 25 Ma ago from  $140\pm 10^\circ\text{C}$  (Fig. 7c). Note that the portions of the cooling histories below  $\sim 130^\circ\text{C}$  and above  $250^\circ\text{C}$  are not constrained by the data. The main discrepancies remaining between the model and the data take place for furnace temperatures above  $1150^\circ\text{C}$  (Fig. 7a), temperatures at which diffusion characteristics are not constrained (see Fig. 7b).

### 3.4. Fission-track analyses

In order to constrain the lower temperature part of V159 time–temperature history, we conducted zircon and apatite fission-track analyses. Owing to the high uranium content of the zircons (900 ppm in average, Table 4) and the related  $\alpha$  damage, the surface of the zircons was easily destroyed during etching. The surface etching rate was higher than normal, resulting in poor exposure of fission tracks. Further, the high uranium concentration resulted in a density of tracks that was not resolvable under a microscope for many crystals. Only 11 crystals could be dated, instead of the 20 usually used. The central zircon fission-track age of V159 is  $77.5\pm 3.9$  Ma ( $\pm 1\sigma$ ) (Table 4; Figs. 7c and 8a).

Table 4  
Fission track data from Song Chay granite sample V159<sup>a</sup>

Mineral	No. of grains counted	Standard track density $\times 10^4 \text{ cm}^{-2}$ (counted)	$\rho_s \times 10^4 \text{ cm}^{-2}$ (counted)	$\rho_i \times 10^4 \text{ cm}^{-2}$ (counted)	U (ppm)	$P(\chi^2)$ (%)	Mean track length ( $\mu\text{m}$ )	Stand dev. ( $\mu\text{m}$ )	No. of lengths	Age $\pm 1\sigma$ (Ma) (central)
Apatite	22	112 (6891)	10.81 (133)	51.46 (633)	6.3	10.1	12 $\pm$ 0.5	2.36	20	33.6 $\pm$ 3.6
Zircon	11	47 (2821)	4012 (2776)	1104 (764)	894	25.5				77.5 $\pm$ 3.9

<sup>a</sup>  $\rho_s$  and  $\rho_i$  represent sample spontaneous and induced track densities;  $P(\chi^2)$  is the probability of obtaining the  $\chi^2$  value for  $\nu$  degrees of freedom, where  $\nu$  is one less than the number of crystals; mean  $\rho_s/\rho_i$  ratio used to calculate ages and uncertainty when  $P(\chi^2) < 5\%$  test. These analyses used the external detector method following the zeta calibration approach (Hurford and Green, 1983) [ $\zeta = 320 \pm 25$  for CN5 (apatite) and  $87 \pm 5$  for CN1 (zircon)].

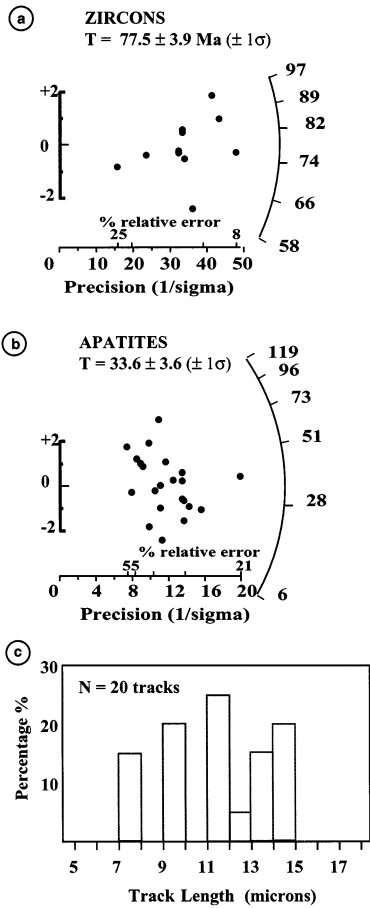


Fig. 8. Fission track data (V159). (a) Zircon radial plot; (b) apatite radial plot; (c) apatite track length distribution histogram.

From experimental studies extrapolated to the geological time scale, current estimates for the zircon fission track partial annealing zone are 390 to 190°C (Yamada et al., 1995). The closure temperature is considered to be about 250  $\pm$  50°C (Hurford, 1986).

Around 77 Ma the temperature given by the K-feldspar model is approximately 170°C (Fig. 7c). Such a temperature is lower than the lower bound for the zircon fission track that we consider at  $\sim$ 200°C. This apparent discrepancy could either result from an incorrect interpretation of the medium part of the K-feldspar age spectrum (e.g. excess argon) or from temperature uncertainties on the K-feldspar model and/or the zircon fission track closure temperature.

For the apatite fission-track system, the partial annealing zone and closure temperature are well constrained as 60 to 120°C and 110  $\pm$  10°C, respectively (e.g. Green et al., 1989; Corrigan, 1991). At temperatures greater than 120°C all tracks are erased and the ‘clock’ is reset.

The central apatite fission-track age is 33.6  $\pm$  3.6 Ma ( $\pm 1\sigma$ ) (Table 4; Fig. 8b). Such an age is in good agreement with the K-feldspar model cooling histories, and seems to indicate that the rapid Tertiary cooling pursued below  $\sim$ 100°C (Fig. 7c).

Further information on the low-temperature history of the sample may be obtained by analysing the apatite fission track length. Unfortunately, owing to the relatively low uranium content (6 ppm on average) only 20 confined track lengths

could be measured (Table 4). The mean track length is  $12 \pm 0.5 \mu\text{m}$  with a standard deviation of  $2.36 \mu\text{m}$ . Owing to the small number of measured track lengths it is impossible to calculate any reliable model time–temperature history. However, a hint of bimodality may be recognized in the track length distribution with the shorter population approximately  $11 \mu\text{m}$  long, and a second group approximately  $14.5 \mu\text{m}$  long (Fig. 8c). Such bimodality suggests that the sample could have experienced a more complex temperature history between  $120^\circ\text{C}$  and the surface temperature. For example, a late moderate re-heating event cannot be ruled out from the apatite fission track or the argon K-feldspar data.

#### 4. Discussion, tectonics implications

From the multi-system geochronology presented above, we have reconstructed the V159  $T-t$  path using the closure temperatures listed in Table 5 (Fig. 9). Combined with our structural and petrographic observations, this cooling history leads us to propose the following first-order  $P-T-t-D$  path for the Song Chay range (Fig. 9).

The high-temperature ductile deformations of zones a and c most probably correspond to local deformations associated with the emplacement of the granite protolith during the Silurian at  $428 \pm 5 \text{ Ma}$ . This age is in good agreement with the regional geology of the rest of Northern

Vietnam, where unmetamorphic Devonian and younger sediments unconformably rest on pre-Devonian low-grade metasediments (Fig. 1) (e.g. Hutchinson, 1989, p. 144). Such a Silurian age is also comparable to the inferred age of many granitic batholiths in the ‘Caledonian’ South China fold belt (Fig. 1b) ( $\gamma 3$ , Academia Sinica, 1976). One of these granites, the Zhuguangshan batholith, yielded two U/Pb zircon ages of  $427 \pm 3$  and  $434 \pm 2 \text{ Ma}$  (Li et al., 1989; Li, 1994). In South-East China the ‘Caledonian’ deformations are marked by a clear angular unconformity between Devonian sandstones and shales, and Ordovician–Silurian folded strata (e.g. Hutchinson, 1989, p. 139). The Song Chay granite thus appears to represent the westernmost prong of the ‘Caledonian’ South China fold and granitic fold belt north of the ASRR shear zone.

The argon and Rb/Sr micas ages taken together with their corresponding closure temperatures are compatible. They seem to indicate a rapid Upper Triassic cooling episode followed by a slower Lower Jurassic one (Fig. 9). From the time of protolith crystallization to the onset of Triassic cooling, rocks could have suffered a regular slow cooling at an average rate of  $\sim 0.5^\circ\text{C/m.y.}$  (curve 1, Fig. 9). Such a cooling path would suggest an absence of a tectonic or metamorphic event between the Silurian and the Upper Triassic. This would contradict the above interpretation of the Song Chay dome as a part of the ‘Caledonian’ South China belt, characterized by Silurian mag-

Table 5  
Summary of geochronology results

Mineral	Method	Age (Ma)	Closure $T$ ( $^\circ\text{C}$ )	Reference
Zircon	U/Pb	$428 \pm 5$ ( $\pm 2\sigma$ )	< 800	Pidgeon and Aftalion (1978), Mezger (1990), Dahl (1997), Lee et al. (1997)
Muscovite	Rb/Sr	$206 \pm 10$ ( $\pm 2\sigma$ )	450–500	Purdy and Jäger (1976), Cliff (1985)
Muscovite	$^{39}\text{Ar}/^{40}\text{Ar}$	$210 \pm 9$ ( $\pm 2\sigma$ )	$390 \pm 45$	Dodson (1973), Hames and Bowring (1994)
Biotite	Rb/Sr	$176 \pm 5$ ( $\pm 2\sigma$ )	300–350	Purdy and Jäger (1976), Harrison and Armstrong (1978)
Biotite	$^{39}\text{Ar}/^{40}\text{Ar}$	$190 \pm 8$ ( $\pm 2\sigma$ )	$320 \pm 40$	Dodson (1973), Harrison and Armstrong (1978), Harrison et al. (1979)
K-feldspar	$^{39}\text{Ar}/^{40}\text{Ar}$	$\sim 35$ to 150	Model cooling histories ( $\sim 130$ to $250^\circ\text{C}$ )	
Zircon	Fission track	$77.5 \pm 3.9$ ( $\pm 1\sigma$ ) (central age)	$250 \pm 50$	Hurford (1986)
Apatite	Fission track	$33.6 \pm 3.6$ ( $\pm 1\sigma$ ) (central age)	$110 \pm 10$	Green et al. (1989), Corrigan (1991)

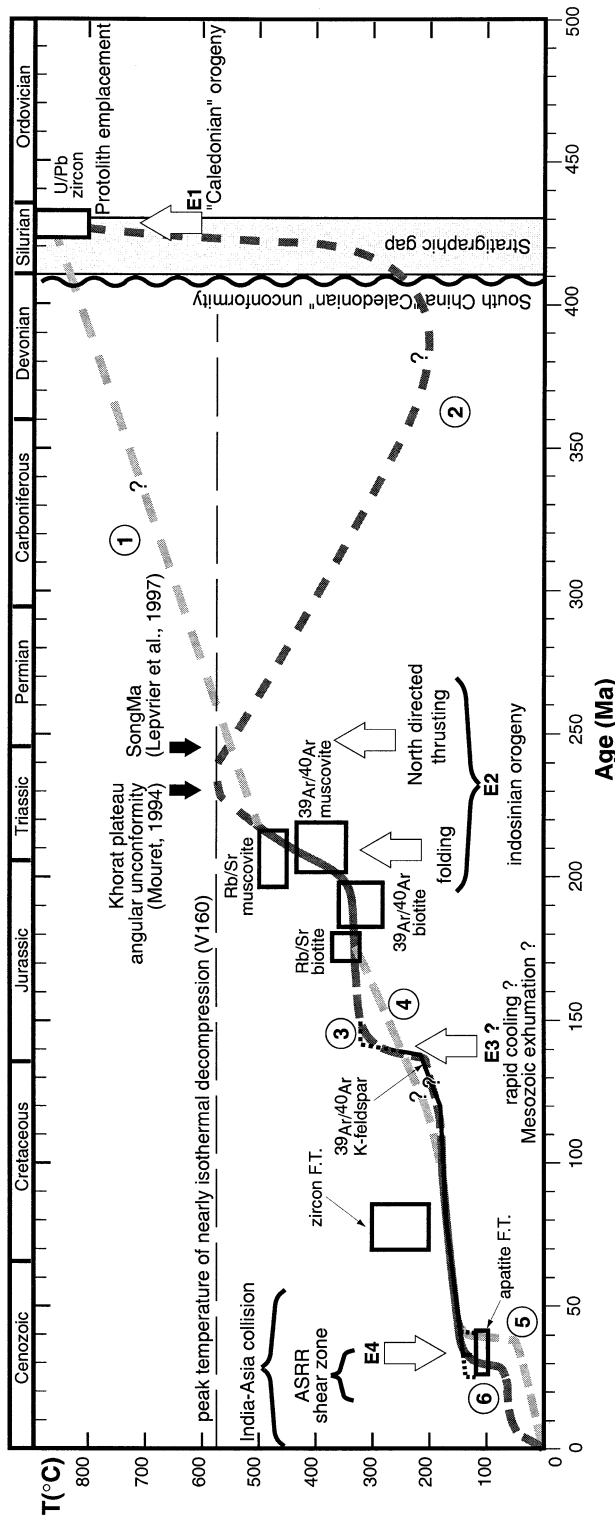


Fig. 9. V159 cooling history from multi-system geochronology. Geochronological data from this study (open boxes at  $2\sigma$  and thin black lines) are plotted together with other geological data. The grey lines represent the assumed cooling histories. Dashed sections indicate possible alternative cooling histories. Dashed numbers refer to text. E1 to E4 refer to possible geological events discussed in the text.

matism and folding, followed by significant exhumation before Lower Devonian sedimentation. Indeed, granitic pebbles are found east of Ha Giang within the Lower Devonian basal conglomerates (Fig. 1) (Tran Van Tri, 1979), suggesting that parts of the Song Chay complex were outcropping at that time. It is thus probable that the Song Chay dome experienced significant cooling and exhumation before the Devonian, and that most evidence for this initial cooling was obliterated by a later heating event (curve 2, Fig. 9). The V160  $P$ – $T$  path suggests that this later heating event culminated at  $\sim 580^\circ\text{C}$  after a nearly isothermal decompression of  $\sim 2$  kbar ( $\sim 6$  km) (Fig. 4). The rapid cooling that follows starts to be documented at  $475 \pm 25^\circ\text{C}$  and  $\sim 210$  Ma (Rb/Sr, muscovite) (Fig. 9). We tentatively interpret such a Permian to Jurassic  $P$ – $T$ – $t$  path as resulting from nappe stacking and doming. North-directed low-angle thrusting, now visible in zone b, first induces limited exhumation and a temperature increase. Then the thrust zone is folded, possibly above the ramp of a deeper thrust, inducing rapid exhumation and cooling. Such large-scale anticlinal folding has been invoked to explain the rapid exhumation and cooling of the Namche-Barwa, Himalaya's eastern syntaxis (Burg et al., 1998). In our interpretation, the Song Chay dome is the internal part of a lower Mesozoic mountain range. The folded Triassic sediments outcropping farther north would correspond to the external part of that mountain range (Fig. 1b). Triassic deformations are widespread in Southeast Asia and are usually affected to the Indosinian orogeny (e.g. Deprat, 1914; Fromaget, 1941) (E2, Fig. 9). In the present-day coordinate the nearest available Indosinian cooling ages come from across the ASRR shear zone in the Song Ma anticlinorium and the Da Nang–Khe Sanh dextral shear zone (Fig. 1). These  $^{39}\text{Ar}/^{40}\text{Ar}$  ages cluster around 245 Ma (Lepvrier et al., 1997) and are thus older than the rapid cooling we document in the Song Chay dome. In other parts of Indochina, reported ages of granitoids and high-grade metamorphism span between 240 and 200 Ma (Liew and Page, 1985; Mahawat et al., 1990; Dunning et al., 1995). In the Khorat plateau, the upper Triassic ( $\sim 230$  Ma) unconformably lies on south-verging folds

(Mouret, 1994). It is difficult to restore the timing and geometry of the Indosinian orogen(s) in SE Asia primarily because of subsequent Tertiary left-lateral movement of several hundreds of kilometres along the ASRR.

The rough upper plateau in the K-feldspar argon age spectrum could suggest that a rapid cooling took place in the Song Chay dome around 140 Ma (curve 3, Fig. 9). It is difficult to correlate such a Jurassic cooling with the geodynamic evolution of Northern Vietnam. During the Jurassic, the proto-Pacific was subducting below the southeastern margin of the South China block, leading to numerous granites and volcanics in the coastal igneous province (Fig. 1b). The main part of this plutonic belt does not outcrop in Northern Vietnam as it seems to abut against the ASRR shear zone near the Hainan island, more than 400 km away from the Song Chay dome. However, some small granites, mapped as Jurassic, intrude the lower Mesozoic cover of the Yangtze platform as well as the northern part of the Song Chay dome (Fig. 1a) ( $n\gamma_5^2$ , Bureau of Geology and Mineral Resources, 1990). Our sampling is far out from the narrow metamorphic aureole of this granite and we do not detect a re-heating event in the V159 thermal history. However, the intrusion of this granite could have been linked with a regional exhumation that would have induced the rapid cooling around 140 Ma (E3, Fig. 9). Alternatively, the K-feldspar upper plateau could be an artefact, due to argon excess or loss, and have no geological meaning. In that case, cooling would have been slow ( $2$ – $3^\circ\text{C}/\text{Ma}$  on average) from Middle Jurassic to Middle Cretaceous (curve 4, Fig. 9). In the absence of other evidence for rapid cooling at  $\sim 140$  Ma, it is difficult to choose between the two possible cooling paths.

The uppermost Cretaceous and Cenozoic thermal history of V159 is constrained by the K-feldspar  $^{39}\text{Ar}/^{40}\text{Ar}$  and the apatite fission tracks data (Fig. 9). The most probable thermal history corresponds to a very slow cooling ( $\sim 0.4^\circ\text{C}/\text{Ma}$ ) that dramatically increases during the Eocene–Oligocene at 41 to 25 Ma (Fig. 9). Around that time, left-lateral deformations occurred in the ASRR shear zone (e.g. Leloup et al., 1995; Zhang and Schärer, 1999). The southern extremity of the

Song Chay complex has probably been affected by the Tertiary ASRR left-lateral deformations (Fig. 1a). This, however, is not the case for most of the complex, where no evidence of such deformations is found. We infer that the Eocene–Oligocene rapid cooling detected in sample V159 more probably relates to exhumation induced by one of the Tertiary compressive deformations that affect the South China block north of the ASRR. In northwest Yunnan, the folded Tiger-leap décollement (T.L. in Fig. 1b) results from two distinct shortening phases whose ages bracket left-lateral shear on the ASRR (Lacassin et al., 1996): Upper Eocene SSW-directed décollement ( $35.9 \pm 0.3$  Ma, Rb/Sr), and Miocene refolding about a north–south axis ( $\sim 17$  Ma,  $^{39}\text{Ar}/^{40}\text{Ar}$  on K-feldspar) (Lacassin et al., 1996). The most obvious structure that could be responsible for a recent exhumation of the Song Chay complex is the east–west Yen Binh thrust fault (Fig. 1a). This would favour a hypothesis of Upper Eocene exhumation of the Song Chay complex during  $\sim$ N–S compression before onset of left-lateral shear on the ASRR and synchronous with SSW movements on the Tiger-leap décollement (curve 5, Fig. 9). However, the age of the rapid cooling is poorly constrained and could be Miocene. At that time, the compression was oriented east–west rather than north–south (e.g. Leloup et al., 1995), and thus incompatible with thrust motion on the Yen Binh fault. One should thus invoke an N–S thrust, for example along the eastern flank of the dome (Fig. 1a). In that case the Yen Binh fault would have formed more recently, as its orientation is compatible with the present-day N–S compression (e.g. Lacassin et al., 1994; Leloup et al., 1995). This would account for the particularly steep topographic gradient of the southern flank of the Song Chay dome. In this second hypothesis, the Cenozoic temperature–time history could have been more complex (curve 6, Fig. 9), as suggested by the apatite fission track length distribution.

## 5. Conclusion

The  $P$ – $T$ – $t$ – $D$  history of the Song Chay dome presented above is preliminary and should be

checked against more field work and petrography/geochronology studies of other samples. However, it yields valuable constraints on the geodynamic evolution of the South China block in Northern Vietnam. Northern Vietnam was affected by pre-Devonian (‘Caledonian’) deformations and magmatism comparable to what is described in the South China fold belt. The Song Chay complex protolith is a granite of that age ( $428 \pm 5$  Ma). Most gneisses now outcropping in the eastern and southern part of the dome probably formed during the granite emplacement. The granite was later affected by low-angle thrusting, with top to the north transport, now visible in the core of the dome. In the Early Jurassic, by  $\sim 200$  Ma, that décollement was folded and cooled down to a temperature of  $\sim 300^\circ\text{C}$ . The Song Chay dome did not suffer penetrative deformations during the Cenozoic. However, it started to cool rapidly from  $\sim 130^\circ\text{C}$  in the Eocene–Oligocene. This cooling could correspond to exhumation by the Yen Binh fault during the Upper Eocene or to two successive exhumation phases due to the two orthogonal compressions (east–west then north–south) that have affected Northern Vietnam since the Oligocene.

Multi-system geochronology thus appears to be a valuable tool to decipher complex geological histories even when applied to a limited number of samples. However, it requires close cooperation between specialists of various geochronological methods and a structural and petrographic control, without which the same temperature history can be interpreted in many different ways. Such a study can later be completed by more systematic analysis that will focus on a given part of the  $P$ – $T$ – $t$ – $D$  path.

## Acknowledgements

We thank Nicolas Arnaud who gave us access to the mass spectrometer and for numerous discussions. Jean Robert Kienast helped us to unravel V160  $P$ – $T$  evolution. The French ‘Ministère des Affaires Etrangères’ provided air plane tickets to P.H.L. and R.L. Oscar Lovera provided the software for K-feldspar argon interpretation. B.

Grasemann and an anonymous reviewer helped us to improve this manuscript with critical comments. This is IPGP contribution no. 1662.

## Appendix A: Analytical procedures

### A.1. *Electronic microprobe mineral analyses*

Mineral analyses were performed with a Cameca Camebax microbeam electronic microprobe at the CAMPARIS analysis centre (Jussieu Campus, France). The accelerating voltage was 15 kV and beam diameter was  $\sim 2 \mu\text{m}$  for feldspars and garnets and  $\sim 10 \mu\text{m}$  for micas.

### A.2. *Multi-system geochronology*

2 kg of the sample V159 were crushed, and mineral separates were obtained using the density separator (Densitest<sup>®</sup>), the Frantz isodynamic magnetic separator, heavy liquids and final selection under binocular microscope.

For the U/Pb analysis, the fractions were selected grain-by-grain to represent the entire range of crystal types present in the population. The zircons selected for U/Pb analysis were euhedral, unbroken, crack-free crystals, translucent and inclusion free. Seven fractions were made using colour (pink), shape and size criteria; their weight ranges from 0.013 to 0.19 mg. Some zircon fractions were mechanically abraded (Krogh, 1982) prior to dissolution in polytetrafluoroethylene (PTFE) Teflon bombs with  $> 50\%$  HF at  $220^\circ\text{C}$  for 2–3 days (Krogh, 1973). Prior to Rb/Sr analyses, feldspar, whole rock and micas were dissolved in two stages at  $150^\circ\text{C}$  ( $> 50\%$  HF and 6 N HCl). U/Pb and Rb/Sr analyses were performed following the isotope dilution method using  $^{205}\text{Pb}$ – $^{235}\text{U}$ – $^{233}\text{U}$  and  $^{85}\text{Rb}$ – $^{84}\text{Sr}$  mixed isotope tracers respectively. Isotope ratios were measured on a Cameca TSN 206 instrument, equipped with a single Faraday collector and a secondary electron multiplier for U, Pb and Rb, and a double Faraday collector for Sr. The decay constants used for U and Rb are those recommended by IUGS (Steiger and Jäger, 1977). For Sr standard NBS 987 an average value of  $^{87}\text{Sr}/^{86}\text{Sr}=0.71024\pm 3$  ( $2\sigma$ ,  $n=$

25) was obtained. Analyses of the NBS 983 standard yield a mean mass fractionation value of  $0.1\pm 0.05\%$ /amu for both the Faraday and secondary electron multiplier systems. Sr ratios were normalized to  $^{86}\text{Sr}/^{88}\text{Sr}=0.1194$ . Total blanks lie around 10–15 pg for Pb and below 1 pg for U, whereas blanks for Rb and Sr are negligible. All zircon analyses were corrected for initial common Pb, the isotopic compositions of which were determined on leached K-feldspars from the same rock sample (Table 1). U/Pb and Rb/Sr calculations were made using the Isoplot 200 program of Ludwig (1992). Analytical uncertainties are listed at  $2\sigma$  and uncertainties in ages as 95% confidence levels.

For argon measurements, 20 mg of K-feldspar and 5 mg of mica were irradiated together with Fish Canyon sanidine flux monitors (FCT,  $27.55\pm 0.08$  Ma, Lanphere and Baadsgaard, 1997) and  $\text{CaF}_2$  and  $\text{K}_2\text{SO}_4$  salts in the Mélusine reactor of the Commissariat à l'Énergie Atomique of Grenoble, France. They were treated by furnace progressive heating; argon isotopic composition was measured at the  $^{40}\text{Ar}/^{39}\text{Ar}$  laboratory in Clermont Ferrand, using a VG3600 mass spectrometer. A particularly long furnace heating schedule, including two-stage isothermal stepwise heating between  $400$  and  $650^\circ\text{C}$  and back cycling, was conducted on K-feldspar in order to retrieve sample diffusion characteristics. During analysis the  $^{39}\text{Ar}$  line blank was always less than 0.14 mV, whereas the  $^{40}\text{Ar}$  line blank was on the order of 90 mV at  $1200^\circ\text{C}$  and 40 mV at ambient temperature.

Fission track ages of apatites and zircons were determined using the external detector method (Hurford and Green, 1983). Apatite grains were mounted on a glass slide, ground, polished and etched in  $6.5\%$   $\text{HNO}_3$  for 50 s at  $20^\circ\text{C}$ , in order to reveal natural fission tracks. Zircons were mounted in Teflon, ground and polished, and etched in the eutectic mixture of NaOH and KOH (Gleadow et al., 1976) at  $210^\circ\text{C}$  for 12 h. The muscovite external detectors were etched in  $40\%$  HF for 40 min at  $20^\circ\text{C}$  to reveal the induced fission tracks. Samples were irradiated at the ANSTO facility, at Lucas Heights, Australia, with a nominal neutron flux of  $1.0\times 10^{16}$  n/cm<sup>2</sup> for apatites and

$1.0 \times 10^{15}$  n/cm<sup>2</sup> for zircons. The ages were calculated following the method described by Hurford (1990), using the zeta calibration method (Hurford and Green, 1983). Durango apatite ( $31.4 \pm 0.5$  Ma) and Fish Canyon Tuff zircons ( $27.55 \pm 0.08$  Ma) (Lanphere and Baadsgaard, 1997) were used as age standards. Fission tracks were counted on the Zeiss microscope, using a magnification of  $1250 \times$  under dry objectives for apatites, and  $1600 \times$  oil immersion for zircons. All ages are central and are quoted at  $\pm 1\sigma$ .

## References

- Academia Sinica, 1976. Geological Map of China, Scale 1: 4 000 000. Geological Publishing House, Beijing.
- Bureau of Geology and Mineral Resources of Yunnan Province, 1990. Regional Geology of Yunnan Province. Geological Memoirs. Geological Publishing House, Beijing, 728 pp.
- Burg, J.P., Nievergelt, P., Oberli, F., Seward, D., Davy, P., Maurin, J.C., Diao, Z., Meier, M., 1998. The Namche Barwa syntaxis: evidence for exhumation related to compressional crustal folding. *J. Asian Earth Sci.* 16, 239–252.
- Cliff, R.A., 1985. Isotopic dating in metamorphic belts. *J. Geol. Soc. London* 142, 97–110.
- Corrigan, J., 1991. Inversion of apatite fission track data for thermal history information. *J. Geophys. Res.* 96, B6, 21 927–21 941.
- Dahl, P.S., 1997. A crystal-chemical basis for Pb retention and fission-track annealing systematics in U-bearing minerals, with implications for geochronology. *Earth Planet. Sci. Lett.* 150, 277–290.
- Deprat, J., 1914. Etude des plissements et des zones d'écrasement de la moyenne et basse rivière noire. *Mém. Serv. Géol. Indochine* 3 (4), 1–59.
- Deprat, J., 1915. Etudes géologiques sur la région septentrionale du Haut Tonkin. *Mém. Serv. Géol. Indochine* 4 (4) 175 pp.
- Dodson, M.H., 1973. Closure temperature in cooling geochronological and petrological systems. *Contrib. Mineral. Petrol.* 40, 259–274.
- Dunning, G.R., Macdonald, A.S., Barr, S.M., 1995. Zircon and monazite U/Pb dating of the Doi Inthanon core complex, northern Thailand: implications for extension within the Indosinian orogen. *Tectonophysics* 251, 197–213.
- Fromaget, J., 1941. L'Indochine française, sa structure géologique, ses roches, ses mines et leurs relations possibles avec la tectonique. *Bull. Serv. Géol. Indochine* 26 (2) 140 pp.
- Gapais, D., 1989. Shear structures within deformed granites: mechanical and thermal indicators. *Geology* 17, 1144–1147.
- General Department of Mines and Geology of the Socialist Republic of Vietnam, 1988. Geological Map of Kampuchea, Laos and Vietnam, scale 1:1000000. General Department of Mines and Geology of the Socialist Republic of Vietnam, Hanoi.
- General Geological Department of the Democratic Republic of Vietnam, 1973. Geological Map of Vietnam (The North Part), Scale 1:1000000. General Geological Department of the Democratic Republic of Vietnam, Hanoi.
- Gleadow, A.J.W., Hurford, A.J., Quaipe, R.D., 1976. Fission track dating of zircons: improved etching techniques. *Earth Planet. Sci. Lett.* 33, 273–276.
- Green, P.F., Duddy, I.R., Laslett, G.M., Hegarty, K.A., Gleadow, A.J.W., Lowering, J.F., 1989. Thermal annealing of fission tracks in apatite, 4. Quantitative modelling techniques and extension to geological timescales. *Chem. Geol.* 79, 155–182.
- Hames, W.E., Bowring, S.A., 1994. An empirical evaluation of the argon diffusion geometry in muscovite. *Earth Planet. Sci. Lett.* 124, 161–167.
- Harrison, T.M., Armstrong, R.L., Clarke, G.K.C., 1978. Thermal models and cooling histories from fission-track, K–Ar, Rb/Sr and U/Pb mineral dates, Northern Coast Pluton Complex British Columbia abstract. In: Short Papers of the Fourth International Conference on Geochronology, Cosmochronology, Isotope Geology. U.S. Geol. Surv., Open-File Rep., pp. 167–170.
- Harrison, T.M., Armstrong, R.L., Naeser, C.W., Harakal, J.E., 1979. Geochronology and thermal history of the coast plutonic complex, near Prince Rupert, British Columbia. *Can. J. Earth Sci.* 16, 400–410.
- Hodges, K.V., Spear, F.S., 1982. Geothermometry, geobarometry and the Al<sub>2</sub>SiO<sub>5</sub> triple point at Mt. Moosilauke, New Hampshire. *Am. Mineral.* 67, 118–134.
- Hoisch, T., 1991. Equilibria within the mineral assemblage quartz + muscovite + biotite + garnet + plagioclase and implications for the mixing properties of octahedrally-coordinated cations in muscovite and biotite. *Contrib. Mineral. Petrol.* 108, 43–54.
- Hurford, A.J., 1986. Cooling and uplift patterns in the Lepontine Alps South Central Switzerland and age of vertical movement on the Insubric fault line. *Contrib. Mineral. Petrol.* 92, 413–427.
- Hurford, A.J., 1990. Standardization of fission-track dating calibration: recommendation by the Fission Track Working Group of the IUGS Subcommittee on Geochronology. *Chem. Geol. (Isot. Geosci. Sect.)* 93, 413–427.
- Hurford, A.J., Green, P.F., 1983. The zeta calibration of fission-track dating. *Isotope Geosci.* 1, 285–317.
- Hutchinson, C.S., 1989. Geological Evolution of SE Asia. Oxford Monographs on Geology and Geophysics 13. Clarendon, Oxford, 368 pp.
- Izokh, E.P., Le Dyn Hyu, Nguyen Van Tien, 1964. New information on magmatic activity in North Vietnam. *Doklady Akademia Nauk SSSR* 155, 96–98.
- Krogh, T.E., 1973. A loss contamination decomposition of zircon and extraction of U and Pb for isotopic age determination. *Geochim. Cosmochim. Acta* 37, 485–494.
- Krogh, T.E., 1982. Improved accuracy of U/Pb zircon ages by

- the creation of more concordant systems using air abrasion technique. *Geochim. Cosmochim. Acta* 46, 637–649.
- Lacassin, R., Tapponnier, P., Leloup, H.P., Phan Trong, T., Nguyen Trong, Y., 1994. Morphotectonic evidence for active movements along the Red-River fault zone. *Proceedings of Conference International Workshop on Seismotectonics and Seismic Hazard in South East Asia*, Hanoi, Vietnam.
- Lacassin, R., Schärer, U., Leloup, P.H., Arnaud, N., Tapponnier, P., Liu, X., Zhang, L.S., 1996. Tertiary deformation and metamorphism SE of Tibet: the folded tiger-leap décollement of NW Yunnan (China). *Tectonics* 15 (2), 605–622.
- Lanphere, M.A., Baadsgaard, H., 1997. The fish canyon tuff: a standard for geochronology. In: *AGU Spring Meeting*, S326G.
- Lee, J.K.W., Williams, I.S., Ellis, D.J., 1997. Pb, U and Th diffusion in natural zircon. *Nature* 390, 159–161.
- Le Goff, E., Ballèvre, M., 1990. Méthodes d'estimation des conditions pression-température dans les orthogneiss: analyse des relations de phases. *C. R. Acad. Sci. Paris* 311, 119–125.
- Leloup, P.H., Lacassin, R., Tapponnier, P., Zhong, D., Liu, X., Zhang, L., Ji, S., Phan Trong, T., 1995. The Ailao Shan–Red River shear zone (Yunnan, China), Tertiary transform boundary of Indochina. *Tectonophysics* 251, 3–84.
- Lepvrier, C., Maluski, H., Nguyen Van Vong, Roques, D., Axente, V., Rangin, C., 1997. Indosinian NW-trending shear zones within the Truong Son belt (Vietnam) <sup>40</sup>Ar–<sup>39</sup>Ar Triassic ages and Cretaceous to Cenozoic overprints. *Tectonophysics* 283, 105–127.
- Li, X., 1994. A comprehensive U/Pb, Sm/Nd, Rb/Sr and <sup>40</sup>Ar/<sup>39</sup>Ar geochronological study on Guidong granodiorite, southeast China: records of multiple tectonothermal events in a single pluton. *Chem. Geol.* 115, 283–295.
- Li, X., Tatsumoto, M., Premo, W.R., 1989. Age and origin of the Tanghu granite, southeast China: results from U/Pb single zircon and Nd isotopes. *Geology* 17, 395–399.
- Liew, T.C., Page, R.W., 1985. U/Pb zircon dating of granitoid plutons from the west coast province of Peninsular Malaysia. *J. Geol. Soc. London* 142, 515–526.
- Lovera, O.M., 1992. Computer programs to model <sup>40</sup>Ar/<sup>39</sup>Ar diffusion data from multidomain samples. *Computers and Geosciences* 18, 789–813.
- Lovera, O.M., Richter, F.M., Harrison, T.M., 1989. The <sup>40</sup>Ar/<sup>39</sup>Ar thermochronology for slowly cooled samples having a distribution of diffusion domain sizes. *J. Geophys. Res.* 94, 17917–17935.
- Lovera, O.M., Richter, F.M., Harrison, T.M., 1991. Diffusion domains determined by <sup>39</sup>Ar released during step heating. *J. Geophys. Res.* 96, 2057–2069.
- Lovera, O.M., Grove, M., Harrison, T.M., Mahon, K.I., 1997. Systematic analysis of K-feldspar <sup>40</sup>Ar/<sup>39</sup>Ar step heating results: I. Significance of activation energy determination. *Geochim. Cosmochim. Acta* 61, 3172–3192.
- Ludwig, K.R., 1992. Isoplot 2.57, a plotting and regression program for radiogenic-isotope data (revision). US Geological Survey Open-File Report 91-445, 38 pp.
- Mahawat, C., Atherton, M.P., Brotherton, M.S., 1990. The Tak batholith Thailand: the evolution of contrasting granite types and implications for tectonic setting. *J. SE Asia Earth Sci.* 4, 11–27.
- Mezger, K., 1990. Geochronology in granulites. In: Vielzeuf, D., Vidal, Ph. (Eds.), *Granulites and Crustal Evolution*. Kluwer, pp. 451–470.
- Mouret, C., 1994. Geological history of northeastern Thailand since the Carboniferous. Relations with Indochina and Carboniferous to early Cenozoic evolution model. In: Angsuwanthana, P.T., Wongwanich, W., Tansathien, S., Wongsomsak, V., Tuyatid, J. (Eds.), *Proceedings of the International Symposium on Stratigraphic Correlation of Southeast Asia*. Department of Mineral Resources, Bangkok, pp. 132–158.
- Pidgeon, R.T., Aftalion, M., 1978. Cogenetic and inherited zircon U/Pb systems in granites: Paleozoic granites of Scotland and England. In: Bowes, D.R., Leake, B.E. (Eds.), *Crustal Evolution in Northwestern Britain and Adjacent Regions*, *Geol. J.* 10, 183–220.
- Powell, R., Holland, T.J.B., 1988. An internally consistent dataset with uncertainties and correlations: 3. Applications to geobarometry, worked examples and a computer program. *J. Metamorphic Geol.* 6, 173–204.
- Purdy, J.W., Jäger, E., 1976. In: K–Ar Ages on Rockforming Minerals from the Central Alps. *Mem. Ist. Geol. Mineral., Padova.*, 1–321.
- Staritskiy, Y.G., Maymin, Y.S., Trafimov, V.A., 1973. Tectonic development of Northern Vietnam. *Int. Geol. Rev.* 15, 1381–1390.
- Steiger, R.H., Jäger, E., 1977. Subcommittee on geochronology: convention on the use of decay constants in geo- and cosmochronology. *Earth Planet. Sci. Lett.* 36, 359–362.
- Tapponnier, P., Peltzer, G., Armijo, R., 1986. On the mechanics of the collision between India and Asia. In: Coward, M.P., Ries, A.C. (Eds.), *Collision Tectonics*. *Geol. Soc. London, Spec. Publ.* 19, 115–157.
- Tapponnier, P., Lacassin, R., Leloup, P.H., Schärer, U., Zhong, D., Liu, X., Ji, S., Zhang, L., Zhong, J., 1990. The Ailao Shan/Red River metamorphic belt: Tertiary left-lateral shear between Indochina and South China. *Nature* 343, 431–437.
- Tran Van Tri 1979. *Geology of Vietnam (North Part)*. Explanation to the 1/1 000 000 Geological Map of Vietnam — North Part. Research Institute of Geology and Mineral Resources, Hanoi. 80 pp.
- Yamada, R., Tagami, T., Nishimura, S., Ito, H., 1995. Annealing kinetics of fission tracks in zircons: an experimental study. *Chem. Geol. (Isot. Geosci. Sect.)* 122, 249–258.
- Yang, Z.Y., Besse, J., 1993. Paleomagnetic study of Permian and Mesozoic sediments from Northern Thailand supports the extrusion model for Indochina. *Earth Planet. Sci. Lett.* 117, 525–552.
- Zhang, L.S., Schärer, U., 1999. Age and origin of magmatism along the Cenozoic Red River shear belt, China. *Contrib. Mineral. Petrol.* 134, 67–85.